



## Effect of Temperature on Poly Crystalline Zinc Oxide thin Film Transistor

S. Naceur, N. Sengouga, M. Labeled, A.F. Meftah

*Laboratory of Metallic and Semiconducting Materials (LMSM), Université de Biskra, B.P. 145, 07000 Biskra RP, Algeria*

\*Corresponding author. [n.sengouga@univ-biskra.dz](mailto:n.sengouga@univ-biskra.dz) (N Sengouga), Tel/Fax +213 33 54 31 99

Received. January 27, 2019. Accepted. March 24, 2019. Published. December 07, 2019.

DOI: <https://doi.org/10.58681/ajrt.19030103>

**Abstract.** The effect of temperature on the electrical characteristics of a on polycrystalline zinc oxide thin film transistor (pc-ZnO TFT ) using numerical simulation is studied. The transfer characteristics of the pc-ZnO TFT were computed. The threshold voltage and the electric field mobility were extracted from these transfer characteristics. The drain current shows Arrhenius-type dependence with temperature. The activation energy varies almost linearly from 0.52 eV at  $V_{GS}=0$  V to 0.05 eV at  $V_{GS}=24$  V. This means that this dependence is very strong in the subthreshold regime while it is inactivated beyond threshold voltage. The threshold voltage and the electric field mobility were also found to be thermally activated. This temperature dependence is attributed to the contribution of the density of states to the channel electrons in the sub-threshold region. However the contribution of DOS beyond threshold voltage is negligible. Furthermore, the threshold voltage was found to be proportional to the electric field mobility. The temperature dependence of the pc-TFT transfer characteristics were qualitatively compared to measurements carried out on pc-ZnO TFTs.

**Keywords.** Poly-crystalline ZnO; TFT; Temperature; TCAD simulation.

### INTRODUCTION

Thin film transistors (TFTs) play an important role in today's display panels due to unique characteristics of oxide semiconductors such zinc oxide (ZnO) (Fortunato et al., 2005; Xu Wang et al., 2016). Oxide semiconductors are widely researched for applications in TFTs because of the relatively low-cost compared the mature a-Si TFT technology (Street, 2009). Although the ZnO TFT performance has been greatly improved, its physical properties is still not well understood. In particular the lack of modeling and simulation of ZnO TFTs (Zhou, et al., 2009 ; Zhang et al., 2011). The advantage of using numerical simulation is that it can

provide information and explain physical phenomena that are difficult to achieve by measurement (Dominguez et al., 2016). Usually in non crystalline semiconductors such as polycrystalline ZnO, a continuous distribution of states (deep and tail) in its gap is assumed to account for the observed characteristics of devices such as TFTs (Gao et al., 2011). Like any semiconductor devices, TFTs are very sensitive to temperature variations and the temperature variation can lead to the understanding of the conduction phenomena. To the authors knowledge a limited work is carried on the effect of temperature on ZnO TFTs (Estrada et al., 2014). In this work, we study the effect of temperature on the current-voltage (I-V) characteristics of a thin film transistor based on polycrystalline zinc oxide (pc-ZnO TFT) to explain the experimental behaviour of the I-V characteristics with temperature. The temperature dependence of the TFT parameters (threshold voltage and the field effect mobility) and their temperature dependence are then extracted from the I-V characteristics.

### THE PC-ZNO TFT STRUCTURE

A three dimensional cross section of the pc-ZnO TFT structure used in this work is shown in figure 1 and is similar to work cited by Estrada et al. (2014). The channel is 20 nm thick pc-ZnO, the substrate is a heavily doped n-type poly-silicon which also acts as a gate, the gate insulator is a 100 nm thick SiO<sub>2</sub> layer, the drain and source ohmic contacts are 5 μm long aluminum (Al). The separation between the source and drain is 30 μm. The width of the TFT is 180 μm.

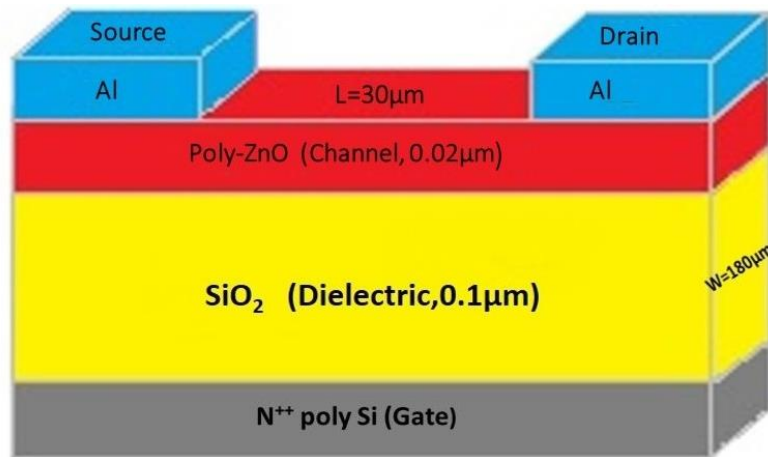


Fig.1. A three dimensional view of the pc-ZnO TFT simulated in this work. The channel is 20 nm thick pc-ZnO, the substrate is a heavily doped n-type poly-silicon which also acts as a gate, the gate insulator is a 100 nm thick SiO<sub>2</sub> layer, the drain and source ohmic contacts are made of aluminum (Al). The separation between the source and drain is 30 μm. The width of the device is 180 μm (not to scale).

The channel is made of pc-ZnO which is a poly-crystalline n-type semiconductor. Its electronic properties (density of states in the gap or DOS) are usually similar to those of amorphous hydrogenated silicon (a-Si:H) and amorphous indium gallium zinc oxide (a-InGaZnO) (Dominguez et al., 2016 ; Kim et al., 2010). The DOS is composed of acceptor like states (near the conduction band) given by the sum of tail states and deep states ( $g_{ct}^A(E) + g_G^A(E)$ ), and donor-like states (near the valence band) given by the sum of tail states and deep states. ( $g_{vt}^D(E) + g_G^D(E)$ ). The total DOS distribution  $g(E)$  is then given by:

$$g(E) = g_{ct}^A(E) + g_G^A(E) + g_{vt}^D(E) + g_G^D(E) \\ = g_{ta} \exp\left(\frac{E-E_C}{E_a}\right) + g_{td} \exp\left(\frac{E_V-E}{E_d}\right) + g_{gd} \exp\left(-\frac{(E-E_D)^2}{\sigma_D^2}\right) + g_{ga} \exp\left(-\frac{(E_A-E)^2}{\sigma_A^2}\right) \quad (1)$$

where  $g_{ta}(cm^{-3}eV^{-1})$  is the effective density at  $E_C$ , and  $E_a$  is the characteristic slope energy of the conduction band-tail states,  $g_{td}(cm^{-3}eV^{-1})$  is the effective density at  $E_V$ , and  $E_d$  is the characteristic slope energy of the valence band-tail states,  $g_{ga}(g_{ga})$ , are the total density ( $cm^{-3}eV^{-1}$ ),  $\sigma_D(\sigma_A)$  the standard deviation and  $E_D(E_A)$  the peak energy of the Gaussian distribution.

## NUMERICAL SIMULATION

Laborious experimental work and/or analytical or qualitative modelling is required to elucidate some observed. Experimental characterisation turns out to be time consuming while analytical modelling can be just mathematical description of the phenomena. Numerical simulation, on the other hand, may be very helpful since it is less time consuming cheaper and above all it is physically based approach. In this work ATLAS is used (Muhr, 2004). In its simplest case it uses the Drift-Diffusion Model (Sze, 1982). This model is based on the Poisson's and steady state continuity equations which are given by:

$$\text{div}(\epsilon \nabla \psi) = -\rho = -q(p - n + n_{tail} - p_{tail} + n_{ga} - p_{gd}) \quad (2)$$

$$0 = \frac{1}{q} \text{div} \vec{J}_n + G_n - R_n \quad (3)$$

$$0 = -\frac{1}{q} \text{div} \vec{J}_p + G_p - R_p \quad (4)$$

where  $\psi$  is the electrostatic potential,  $\epsilon$  is the local permittivity,  $\rho$  is the local space charge density,  $n$  and  $p$  are the free carrier's densities, and  $n_{tail}$ ,  $p_{tail}$ ,  $n_{ga}$ ,  $p_{gd}$  (the DOS constituents) are given by:

$$n_{tail} = \int_{E_V}^{E_C} g_{ct}^A(E) f_{ct}^n(E) dE$$

$$p_{tail} = \int_{E_V}^{E_C} g_{vt}^D(E) f_{vt}^p(E) dE$$

$$n_{ga} = \int_{E_V}^{E_C} g_G^A(E) f_{AG}^n(E) dE$$

$$p_{gd} = \int_{E_V}^{E_C} g_G^D(E) f_{DG}^p(E) dE$$

where  $f_{ct}^n(E)$ ,  $f_{AG}^n(E)$  are the ionization probabilities of the acceptor tail and Gaussian states, respectively, and  $f_{vt}^p(E)$ ,  $f_{DG}^p(E)$  are the ionization of the donor states (tail and Gaussian). At the steady state, these ionization probabilities are given by the Shockley-Read-Hall (SRH) model (Shockley and Read, 1952; Hall, 1952) :

$$f_{ct}^n(E) = \frac{v_{th}^n \sigma_{nc} n + v_{th}^p \sigma_{pc} n_i e^{\frac{E_i - E}{k_B T}}}{v_{th}^n \sigma_{nc} \left( n + n_i e^{\frac{E - E_i}{k_B T}} \right) + v_{th}^p \sigma_{pc} \left( p + n_i e^{\frac{E_i - E}{k_B T}} \right)}$$

$$f_{AG}^n(E) = \frac{v_{th}^n \sigma_{ng}^a n + v_{th}^p \sigma_{pg}^a n_i e^{\frac{E_i - E}{k_B T}}}{v_{th}^n \sigma_{ng}^a \left( n + n_i e^{\frac{E - E_i}{k_B T}} \right) + v_{th}^p \sigma_{pg}^a \left( p + n_i e^{\frac{E_i - E}{k_B T}} \right)}$$

$$f_{vt}^p(E) = \frac{v_{th}^p \sigma_{pv} p + v_{th}^n \sigma_{nv} n_i e^{\frac{E - E_i}{k_B T}}}{v_{th}^n \sigma_{nc} \left( n + n_i e^{\frac{E - E_i}{k_B T}} \right) + v_{th}^p \sigma_{pc} \left( p + n_i e^{\frac{E_i - E}{k_B T}} \right)}$$

$$f_{DG}^p(E) = \frac{v_{th}^p \sigma_{pg}^d p + v_{th}^n \sigma_{ng}^d n_i e^{\frac{E - E_i}{k_B T}}}{v_{th}^n \sigma_{ng}^d \left( n + n_i e^{\frac{E - E_i}{k_B T}} \right) + v_{th}^p \sigma_{pg}^d \left( p + n_i e^{\frac{E_i - E}{k_B T}} \right)}$$

where  $v_{th}^n$  is the electron thermal velocity and  $v_{th}^p$  is the hole thermal velocity,  $n_i$  is the intrinsic carrier concentration.  $\sigma_{nc}$  and  $\sigma_{ng}^a$  are the electron capture cross-section for the acceptor tail and Gaussian states respectively.  $\sigma_{pc}$  and  $\sigma_{pg}^a$  are the hole capture cross-sections

for the acceptor tail and Gaussian states respectively and  $\sigma_{nv}$ ,  $\sigma_{ng}^d$ ,  $\sigma_{pv}$ , and  $\sigma_{pg}^d$  are the equivalents for donors states.

$\bar{J}_n$  and  $\bar{J}_p$  are the electron and hole current densities,  $G_n$  and  $G_p$  are the generation rates for electrons and holes which are neglected in this study,  $R_n$  and  $R_p$  are the total recombination rates for electrons and holes in Gaussian and tail states, and  $q$  is the electron charge.  $R_n$  and  $R_p$  are assumed to be the same and given by Meftah et al. (2004).

$$R_n = R_p = \int_{E_V}^{E_C} (np - n_i^2) \left\{ \left[ \frac{v_{th}^n v_{th}^p \sigma_{pc} \sigma_{nc} g_{ct}^A(E)}{v_{th}^n \sigma_{nc} \left( n + n_i e^{\frac{E-E_i}{k_B T}} \right) + v_{th}^p \sigma_{pc} \left( p + n_i e^{\frac{E_i-E}{k_B T}} \right)} \right] + \right. \\ \left. \left[ \frac{v_{th}^n v_{th}^p \sigma_{pv} \sigma_{nv} g_{vt}^D(E)}{v_{th}^n \sigma_{nv} \left( n + n_i e^{\frac{E-E_i}{k_B T}} \right) + v_{th}^p \sigma_{pv} \left( p + n_i e^{\frac{E_i-E}{k_B T}} \right)} \right] + \left[ \frac{v_{th}^n v_{th}^p \sigma_{pg}^a \sigma_{ng}^a g_G^A(E)}{v_{th}^n \sigma_{ng}^a \left( n + n_i e^{\frac{E-E_i}{k_B T}} \right) + v_{th}^p \sigma_{pg}^a \left( p + n_i e^{\frac{E_i-E}{k_B T}} \right)} \right] + \right. \\ \left. \left[ \frac{v_{th}^n v_{th}^p \sigma_{pg}^d \sigma_{ng}^d g_G^D(E)}{v_{th}^n \sigma_{ng}^d \left( n + n_i e^{\frac{E-E_i}{k_B T}} \right) + v_{th}^p \sigma_{pg}^d \left( p + n_i e^{\frac{E_i-E}{k_B T}} \right)} \right] \right\} dE$$

## RESULTS AND DISCUSSION

The electrical characteristics are calculated following the specified physical structure and bias conditions. Of interest to the present work, the current-voltage characteristics are calculated for different temperatures. The parameters of this model are presented in Table 1. Other values are set to the default values of ATLAS for pc-ZnO.

Table 1. The parameters of the DOS model in pc-ZnO used in this work.

Parameter	Value
Electron affinity	4.2 eV
Dielectric constant	8.5
Electron mobility	10 cm <sup>2</sup> /V.s
Hole mobility	1.5 cm <sup>2</sup> /V.s
Effective conduction band states	2.5 10 <sup>18</sup> cm <sup>-3</sup>
Effective valence band states	2.5 10 <sup>18</sup> cm <sup>-3</sup>
Energy gap at 300K,	3.4 eV
Density of acceptor-like tail states	1.05 10 <sup>16</sup> cm <sup>-3</sup> .eV <sup>-1</sup>
Density of donor-like tail states	1.05 10 <sup>15</sup> cm <sup>-3</sup> .eV <sup>-1</sup>
Characteristic decay energy acceptor-like tail states	0.05 eV
Characteristic decay energy donor-like tail states	0.1 eV
Capture cross section of electron and hole states	4.0 10 <sup>-15</sup> cm <sup>2</sup>

The simulated transfer characteristics  $I_D = f(V_{GS})$  of the TFT for different temperatures ranging from 300 to 400 K are shown in figure 2 on linear (a) and logarithmic (b) scales.

It is clear that the temperature does not have the same effect in the different segments of the transfer characteristics. In the sub-threshold voltage the current is thermally activated while it is insensitive above the threshold voltage. To see the activated current with temperature the Arrhenius plot of the normalized current  $I/I_{298}$  is presented in figure 3 in the sub-threshold voltage (a), just on the onset of the threshold voltage (b) and well beyond threshold voltage (c).  $I_{298}$  is the current at 298 K (evaluated by ATLAS). This behavior may be due to the fact

that the contribution of the DOS to the electrons in the pc-ZnO channel increases with increasing temperature in the sub-threshold voltage region. As the voltage reaches the threshold this contribution is saturated as the accumulation of electrons in the channel of the TFT is fully achieved. It may also worth to note that well beyond threshold voltage, the behavior with gate voltage is reversed, that it increases with increasing voltage. This may be due to the completion of the contribution from the DOS and the intrinsic electrons of the semiconductor.

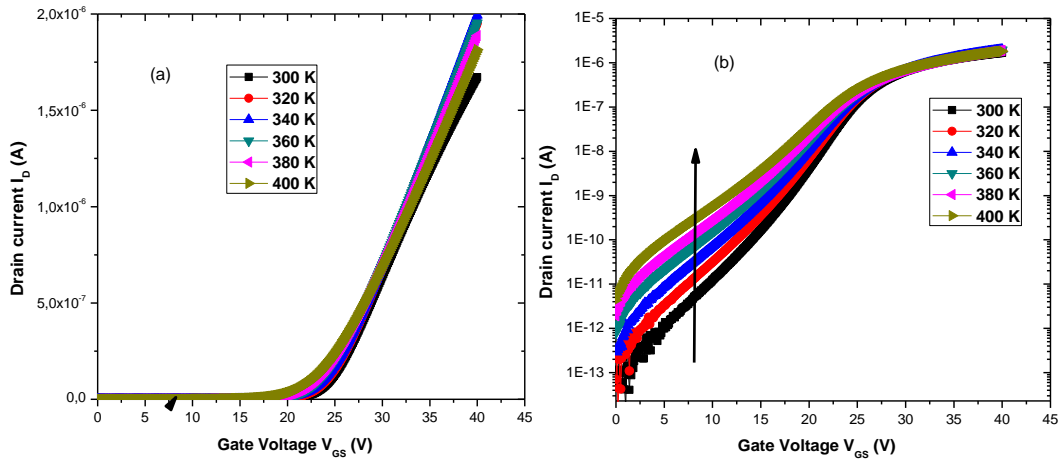


Fig.2. The simulated transfer characteristics  $I_D = f(V_{GS})$  of the TFT for different temperatures ranging from 300 to 400 K on linear (a) and logarithmic (b) scales.

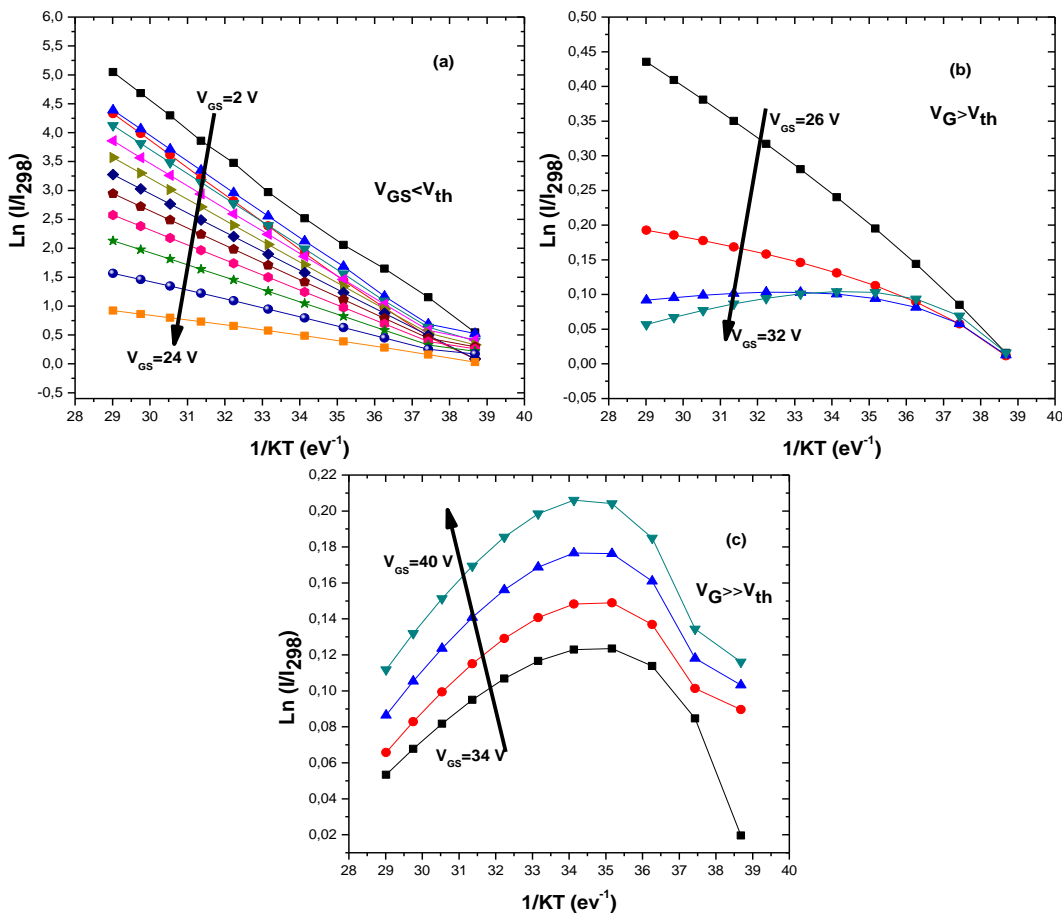


Fig.3. The Arrhenius plot of the normalized current  $I/I_{298}$ . (a) in the sub-threshold voltage, (b) just on the onset of the threshold voltage and (c) well beyond threshold voltage.  $I_{298}$  is the current at 298 K.

It is also clear that the activation energy is not the same in the different segments of the characteristics. Figure 4 presents the activation energies of the current at different segments of the  $I_D = f(V_{GS})$  transfer characteristics of the TFT.

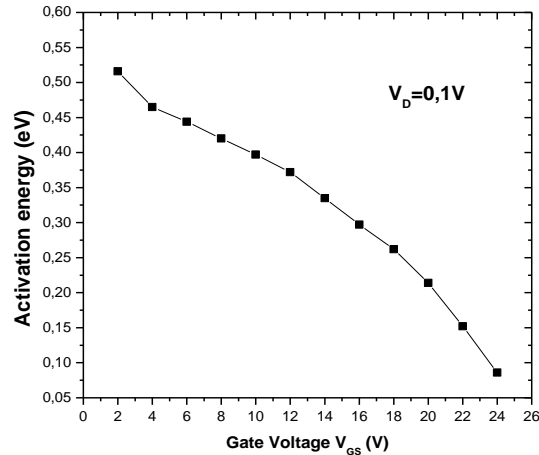


Fig.4. The evaluated activation energy versus the gate voltage.

The activation energy decreases with increasing gate voltage. The high values of the activation energy at low temperatures may be due to the fact that conduction mechanism is dominated by the intrinsic contribution. As the temperature increases the DOS contribution increases leading to shallower activation energy of the current.

The extracted field effect mobility and the threshold voltage from the transfer characteristics  $I_D = f(V_{GS})$  of the pc-ZnO TFT for different temperatures are shown in figure 5.

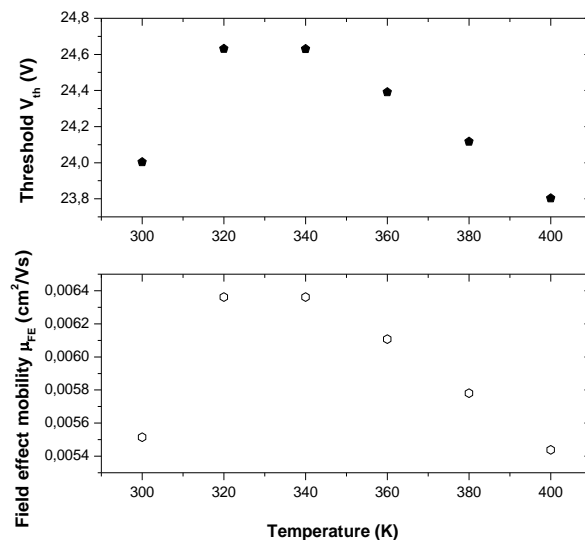


Fig.5. The effect of temperature on the field effect mobility and the threshold voltage extracted from the transfer characteristics  $I_D = f(V_{GS})$  of the pc-ZnO TFT of figure 2.

The extracted field effect mobility and the threshold voltage are also temperature dependence. The mobility increases initially with increasing temperature; it then peaks before starting to decrease. This behavior may also be attributed to the contribution of the DOS to the electrons

in the channel. At relatively low temperatures, the contribution of the DOS is negligible which leads to the increase of the mobility. As the temperature increases; the contribution of the DOS increases leading to increasing collisions and hence a decrease in the mobility. Since the threshold voltage is proportional to the electric field mobility, it is expected that it follows the same pattern, which the case here.

## CONCLUSION

A numerical simulation is carried using ATLAS to study the effect of temperature on the transfer characteristics of a poly crystalline zinc oxide thin film transistor (pc ZnO TFT). The drain current shows an Arrhenius-type dependence on temperature. The activation energy decreases almost linearly with increasing gate voltage. This means that dependence is very strong in the subthreshold regime with while it is inactivated beyond threshold voltage. The extracted threshold voltage and the electric field mobility were also found to be thermally activated. This temperature dependence may be due to the contribution of the density of states to the conduction in channel at the sub-threshold region. On the other hand, the contribution of these DOS is negligible beyond threshold voltage. Furthermore, the threshold voltage was found to be proportional to the electric field mobility. The temperature dependence of the pc-TFT transfer characteristics were qualitatively compared to measurements carried out on crystalline ZnO TFTs (Estrada et al., 2014).

## REFERENCES

- Dominguez, M. A., Alcantara, S., & Soto, S. (2016). Physically-based simulation of zinc oxide thin-film transistors: Contact resistance contribution on density of states. *Solid-State Electronics*, 120. <https://doi.org/10.1016/j.sse.2016.03.006>
- Estrada, M., Gutierrez-Heredia, G., Cerdeira, A., Alvarado, J., Garduño, I., Tinoco, J., Mejia, I., & Quevedo-Lopez, M. (2014). Temperature dependence of the electrical characteristics of low-temperature processed zinc oxide thin film transistors. *Thin Solid Films*, 573. <https://doi.org/10.1016/j.tsf.2014.10.092>
- Fortunato, E. M. C., Barquinha, P. M. C., Pimentel, A. C. M. B. G., Gonçalves, A. M. F., Marques, A. J. S., Pereira, L. M. N., & Martins, R. F. P. (2005). Fully transparent ZnO thin-film transistor produced at room temperature. *Advanced Materials*, 17(5). <https://doi.org/10.1002/adma.200400368>
- Gao, H. X., Hu, R., & Yang, Y. T. (2011). Modeling of polycrystalline ZnO thin-film transistors with a consideration of the deep and tail states. *Chinese Physics B*, 20(11). <https://doi.org/10.1088/1674-1056/20/11/116803>
- Hall, R. N. (1952). Power rectifiers and transistors\*. *Proceedings of the IRE*, 40(11). <https://doi.org/10.1109/JRPROC.1952.273990>
- Hossain, F. M., Nishii, J., Takagi, S., Ohtomo, A., Fukumura, T., Fujioka, H., Ohno, H., Koinuma, H., & Kawasaki, M. (2003). Modeling and simulation of polycrystalline ZnO thin-film transistors. *Journal of Applied Physics*, 94(12). <https://doi.org/10.1063/1.1628834>
- Kim, C. E., Cho, E. N., Moon, P., Kim, G. H., Kim, D. L., Kim, H. J., & Yun, I. (2010). Density-of-states modeling of solution-processed InGaZnO thin-film transistors. *IEEE Electron Device Letters*, 31(10). <https://doi.org/10.1109/LED.2010.2061832>
- Meftah, A. M., Meftah, A. F., Hiouani, F., & Merazga, A. (2004). Numerical simulation of the defect density influence on the steady state response of a silicon-based p-i-n cell. *Journal of Physics Condensed Matter*, 16(12). <https://doi.org/10.1088/0953-8984/16/12/009>
- Muhr, T. (2004). ATLAS TI 5.0 users Guide. *Management in Education*.
- Shockley, W., & Read, W. T. (1952). Statistics of the recombinations of holes and electrons. *Physical Review*, 87(5). <https://doi.org/10.1103/PhysRev.87.835>

- Street, R. A. (2009). Thin-film transistors. *Advanced Materials*, 21(20). <https://doi.org/10.1002/adma.200803211>
- Wang, X., Zhang, Y., Lu, C., & Mao, Z. (2016). Power efficient SRAM design with integrated bit line charge pump. *AEU - International Journal of Electronics and Communications*, 70(10). <https://doi.org/10.1016/j.aeue.2016.08.002>
- Zhang, A., Zhao, X. R., Duan, L. B., Liu, J. M., & Zhao, J. L. (2011). Numerical study on the dependence of ZnO thin-film transistor characteristics on grain boundary position. *Chinese Physics B*, 20(5). <https://doi.org/10.1088/1674-1056/20/5/057201>
- Zhou, Y. M., He, Y. G., Lu, A. X., & Wan, Q. (2009). Simulation of grain boundary effect on characteristics of ZnO thin film transistor by considering the location and orientation of grain boundary. *Chinese Physics B*, 18(9). <https://doi.org/10.1088/1674-1056/18/9/057>